Electronic Supplementary Material (ESI) for Physical Chemistry Chemical Physics.

SUPPORTING INFORMATION

Micro-spectroscopy of KUST-1 Metal-Organic Framework Crystals Loaded with Tetracyanoquinodimethane: Effects of Water on Host-Guest Chemistry and Electrical Conductivity

Miguel Rivera-Torrente,[a] Matthias Filez,[a] Christian Schneider,[b] Ewout C. van der Feltz,[a] Konrad Wolkersdörfer,[c] Dereje H. Taffa,[c] Michael Wark,[c] Roland A. Fischer[b] and Bert M. Weckhuysen*[a]

a. Inorganic Chemistry and Catalysis, Debye Institute for Nanomaterials Science, Utrecht University, Universiteitsweg 99, 3584 CG Utrecht, The Netherlands.
b. Department of Chemistry, Technische Universität München, Lichtenbergstraße 4, 85748 Garching, Germany.
c. Institute of Chemistry, Chemical Technology 1, Carl von Ossietzky Universität Oldenburg, Carl-von-Ossietzky Straße 9-11, 26129 Oldenburg, Germany

TABLE OF CONTENTS

1. Methods and Data Analysis

Principal component analysis (PCA) was carried out with the Matlab R2018a software package (Mathworks). PCA was done by *K*-means clustering of pixels with similar spectral features, resulting into Voronoi cells grouped in four different clusters (colour-coded as shown in Figures 2 and 6 in the main text).

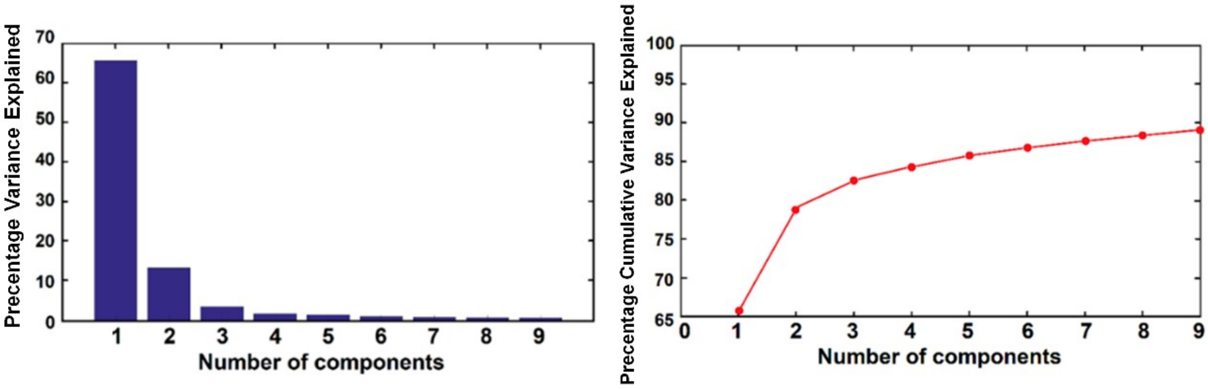

Figure S1. Scree tests and Cumulative Variance Explained (CVE) of each principal component of the Principal Component Analysis (PCA) used for the Raman microscopy analysis.

In Figure S2, the first nine principal components of the PCA analysis carried out for the maps, depicted in Figures 2 and S3, are shown. As it can be noted, most of the spectral information is present in the first few components. This was due to the high intensity of cosmic ray noise that occurs during the spectral acquisition, thus rendering PCA as an extremely useful tool for our purpose.

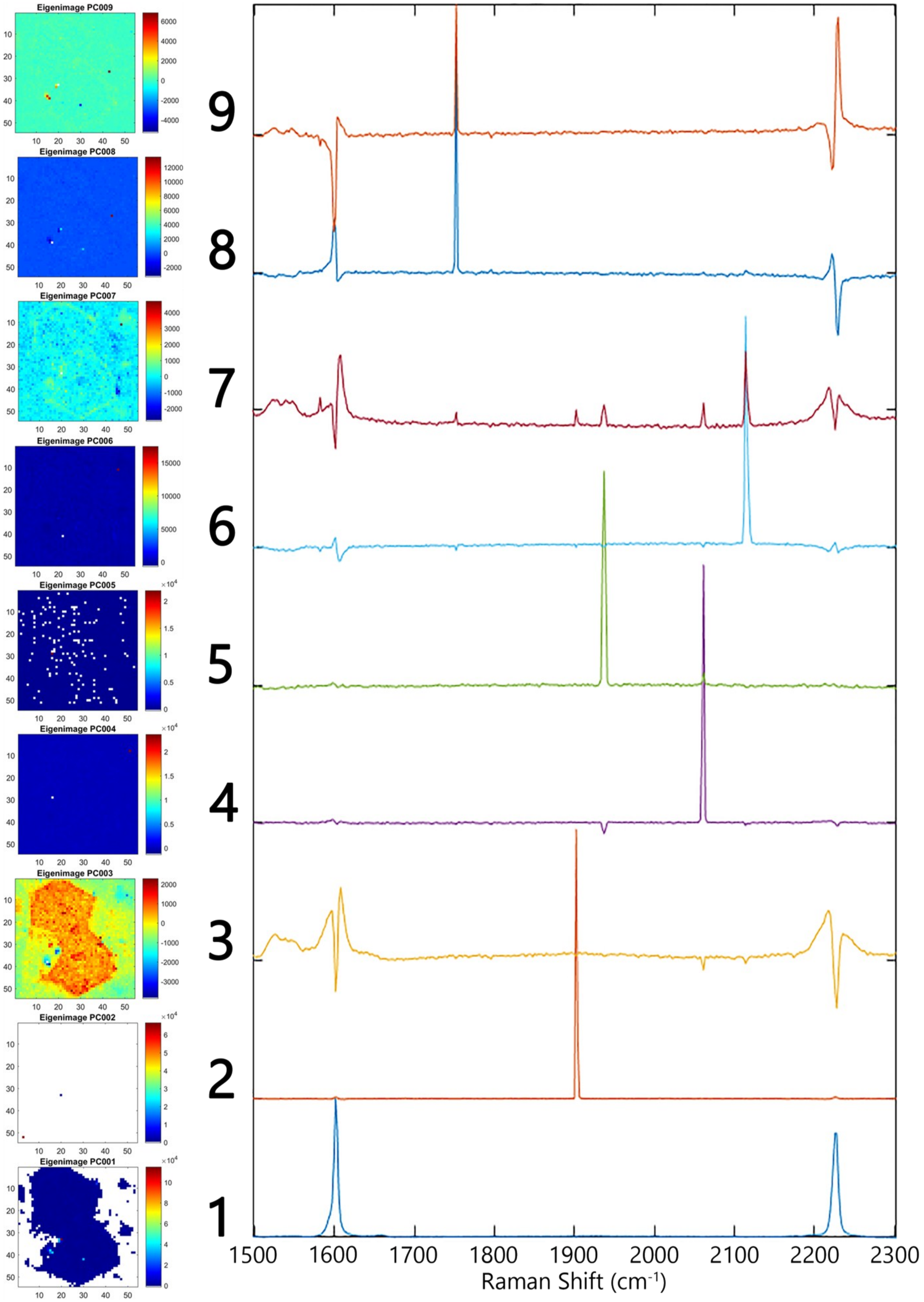

Figure S2. Eigen images and associated spectra for each component of the Principal Component Analysis (PCA) applied on the Raman microscopy maps obtained for the second crystal, as shown in Figures 2 and S3.

2. Raman Spectroscopy of Pure Compounds and Micro-spectroscopic Analysis of a Second TCNQ@HKUST-1 Crystal

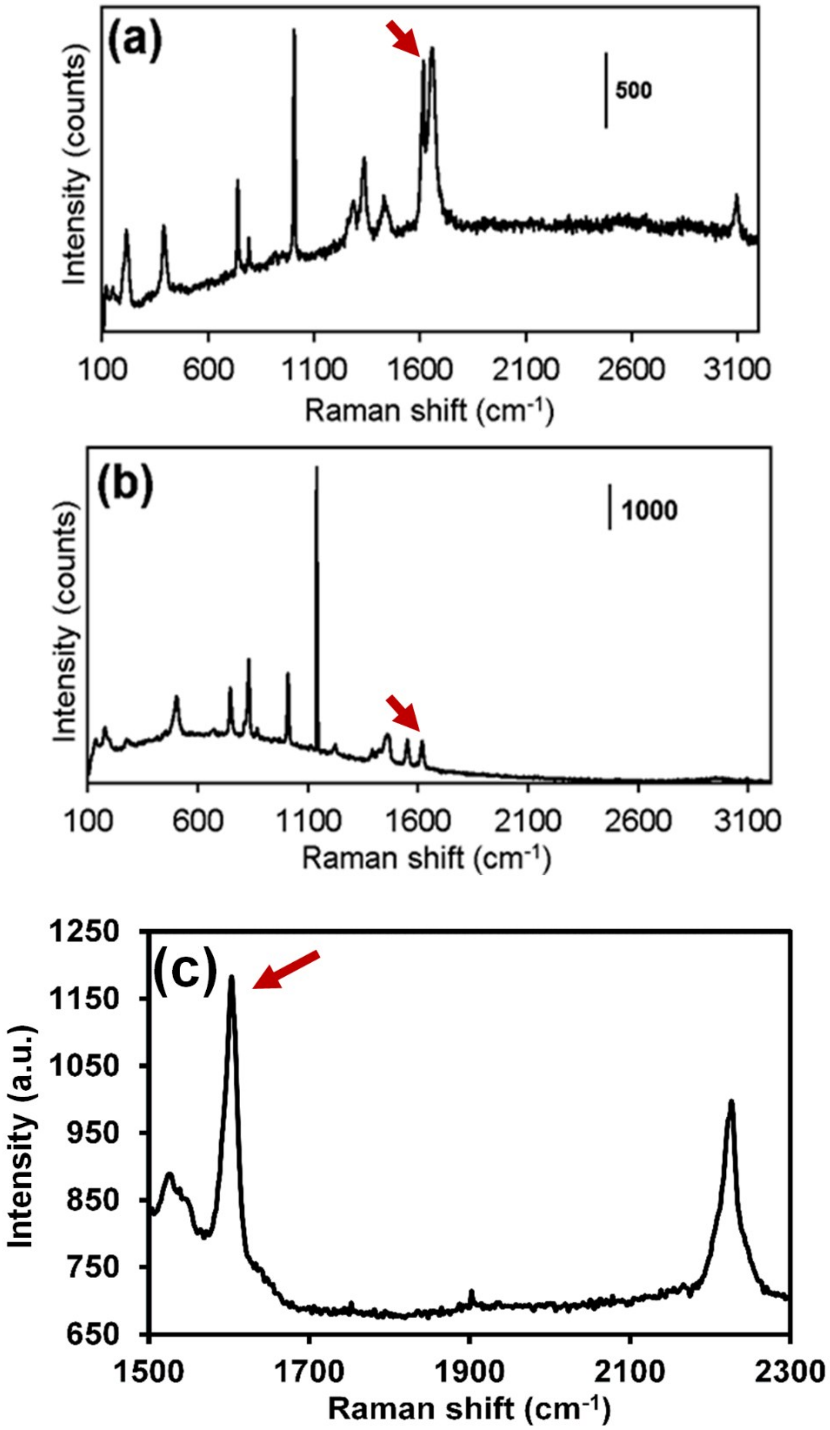

Figure S3. Raman spectrum of (a) pure 1,3,5-benzeneticarboxylic acid and (b) parent HKUST-1 crystals. Note the presence of the C=C aromatic stretch at 1605 cm^{-1} in both spectra (red arrows). (c) Average Raman spectrum of all the pixels mapped for the second crystal showing the bands corresponding to C=C (1605 cm^{-1}) and C≡N (2226 cm^{-1}) stretching modes. Note that the small feature at *ca.* 1900 cm^{-1} is due to the presence of some cosmic ray contributions that were not filtered by PCA.

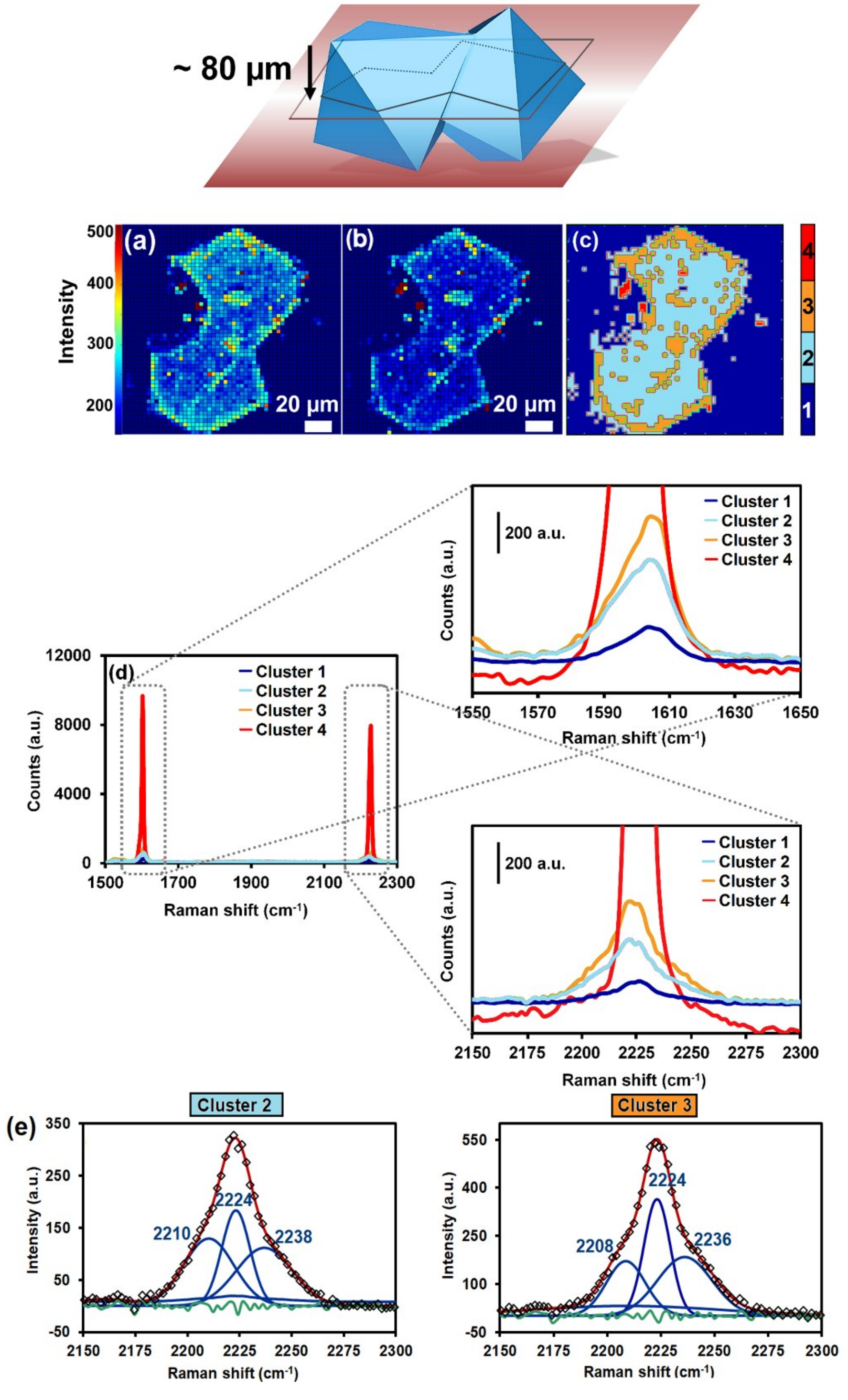

Figure S4. (Top) Scheme showing the cross-section of two intertwined, octahedral HKUST-1 crystals, loaded with TCNQ, and probed with the Raman laser at a depth of *Z* ~ 80 µm. (Bottom) Raman maps of a second crystal showing a similar trend with aggregates around the crystal edges. Signal-to-baseline ratio maps of the Raman bands at (a) 1605 cm^{-1} (corresponding to the C=C aromatic stretching vibration); and at (b) 2226 cm^{-1} (corresponding to the C≡N stretching vibration) of TCNQ. (c) Different spectral clusters obtained from Principal Component Analysis (PCA) of the 1500-2300 cm^{-1} region showing different intensities throughout the two adjacent TCNQ@Cu_3BTC_2 crystals. (d) Raman spectra corresponding to each cluster of the map in (c). (e) Deconvolution of the band corresponding to the nitrile stretch in clusters 2 and 3 of the average spectra shown in (d). The green line corresponds to the residual of the Nedler-Mead simplex algorithm used.

3. *In-situ* X-ray Diffraction (XRD) of Pristine HKUST-1 Crystals

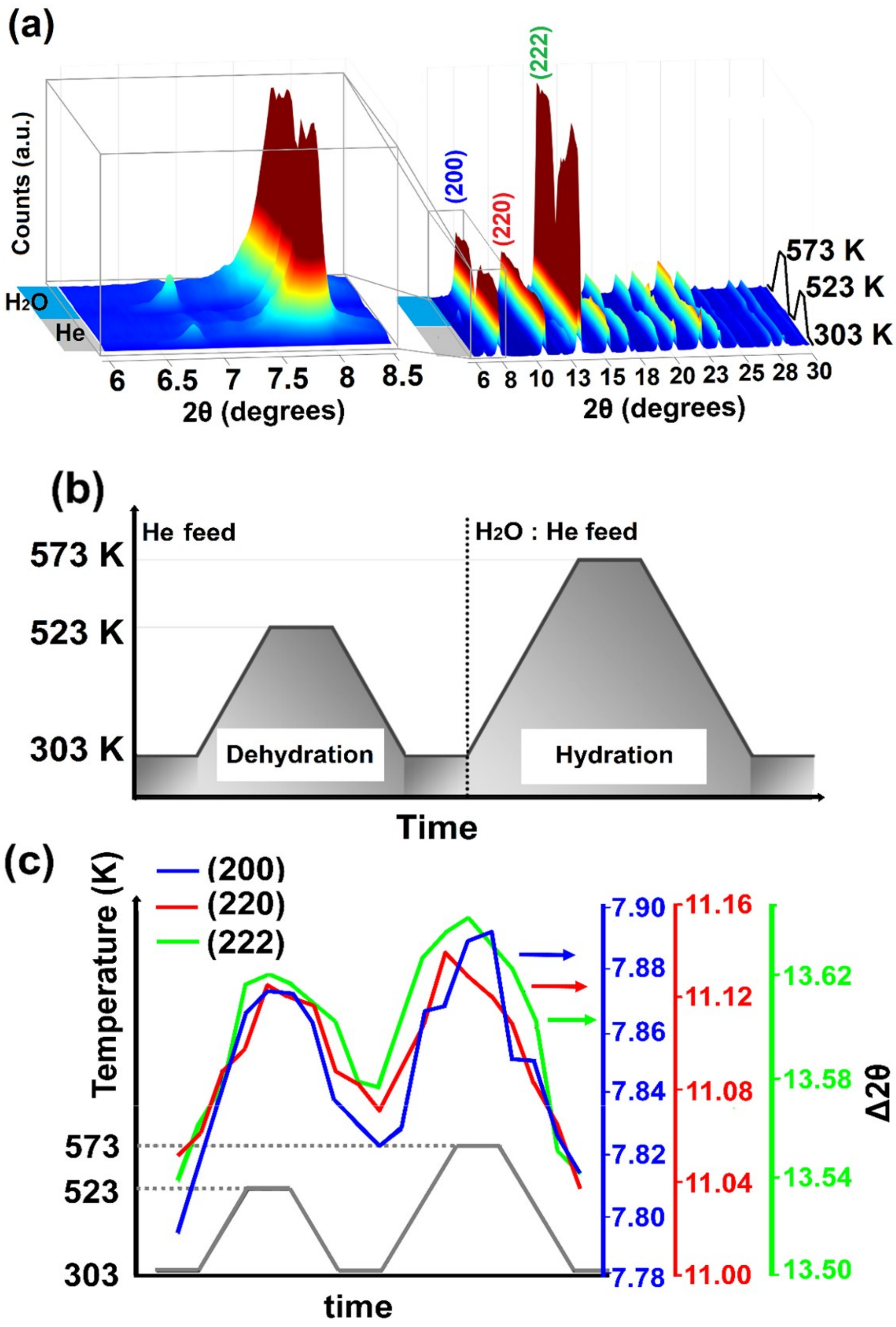

Figure S5. (a) Evolution of the intensities of the X-Ray Diffraction (XRD) peaks of the TCNQ@HKUST-1 host-guest composite material over time under dynamic conditions, as shown in the scheme (b). Dehydration of the crystals results in higher lattice parameter *d* of the (200), (220) and (222) plane reflections, as evidenced by the shift shown in (c). Dosing of water vapor at higher temperatures does not significantly affect the HKUST-1 lattice.

4. Water Adsorption-Desorption Experiments of TCNQ@HKUST-1

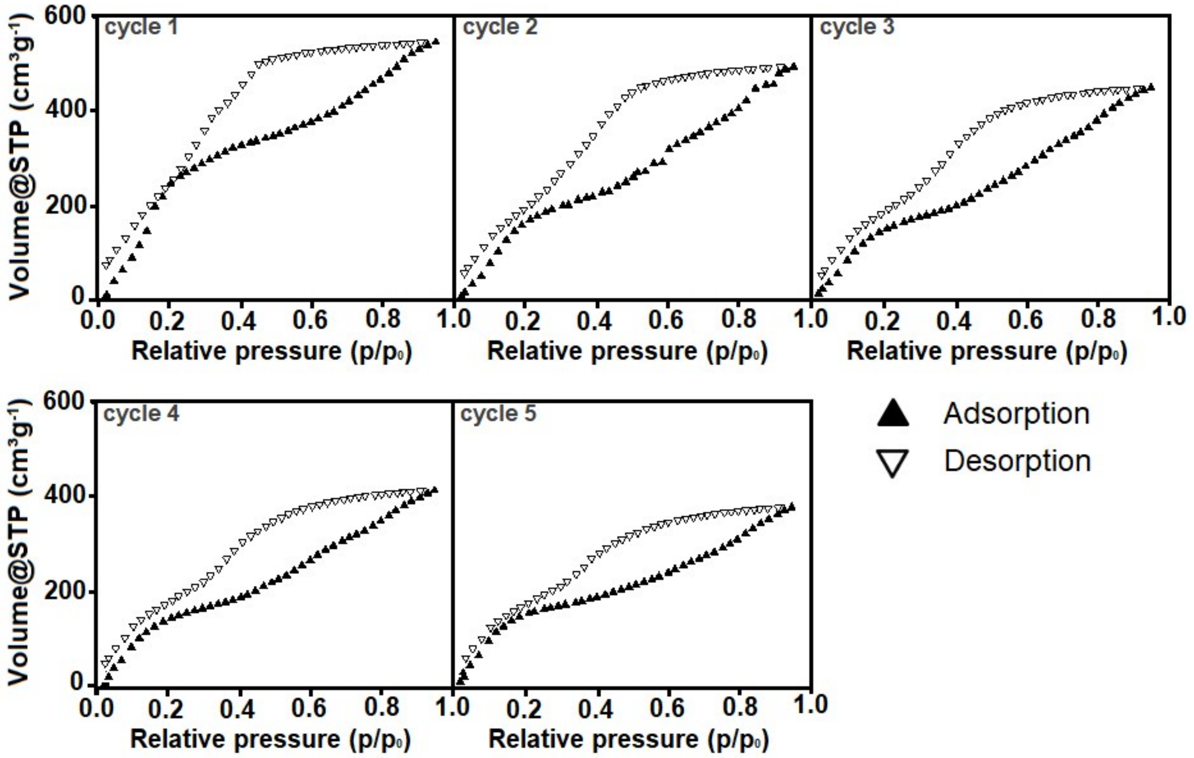

Fig S6. Water adsorption-desorption cycles of the TCNQ@HKUST-1 host-guest composite material measured at 298 K. STP stands for standard pressure and temperature (273 K, 1 bar).

5. X-ray Diffraction (XRD) of TCNQ@HKUST-1 after Exposure to Air Atmosphere

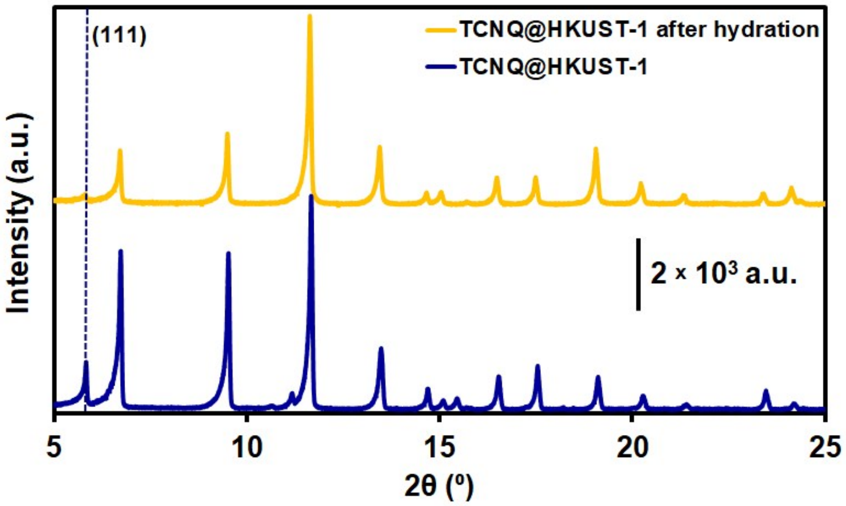

Figure S7. Powder XRD of TCNQ@HKUST-1 before (blue) and after (yellow) exposure to air atmosphere. Dashed line at 5.8 ° indicates the (111) reflection originating from TCNQ ordered within the pores.

6. Current *vs.* Voltage (I-V) Graphs of TCNQ@HKUST-1 Powder

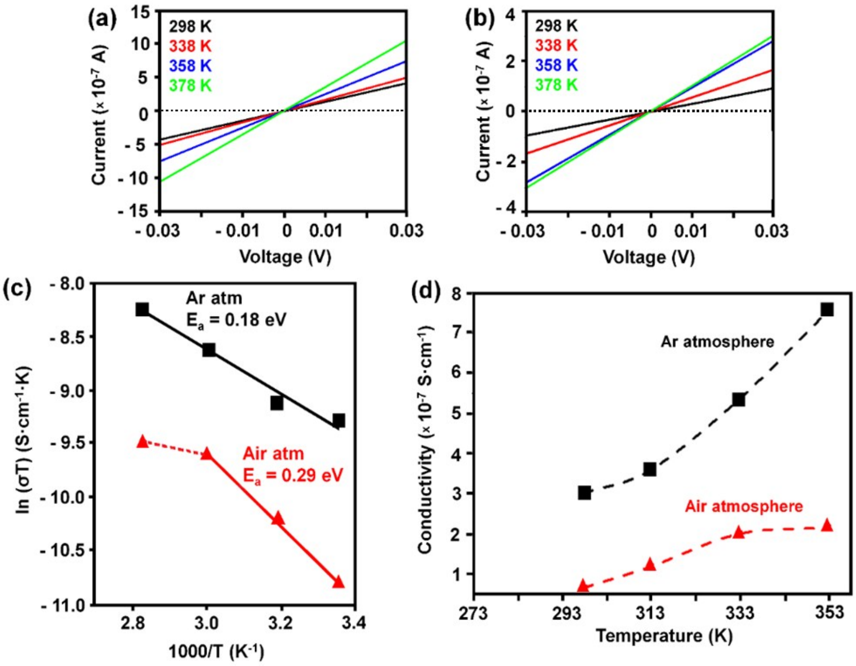

Figure S8. I-V graphs of the TCNQ@HKUST-1 host-guest composite material under (a) Ar and (b) ambient atmospheres at different temperatures: 298 (black), 318 (red), 338 (blue) and 358 K (green). Note the different y-axis scales when comparing conductivity. (c) Arrhenius plot *ln (σT) vs. 1/T* of the conductivity measurements showing higher activation energy for the material exposed to air and (d) evolution of the conductivity at different temperatures under Ar (black squares) and ambient (red triangles) atmospheres.

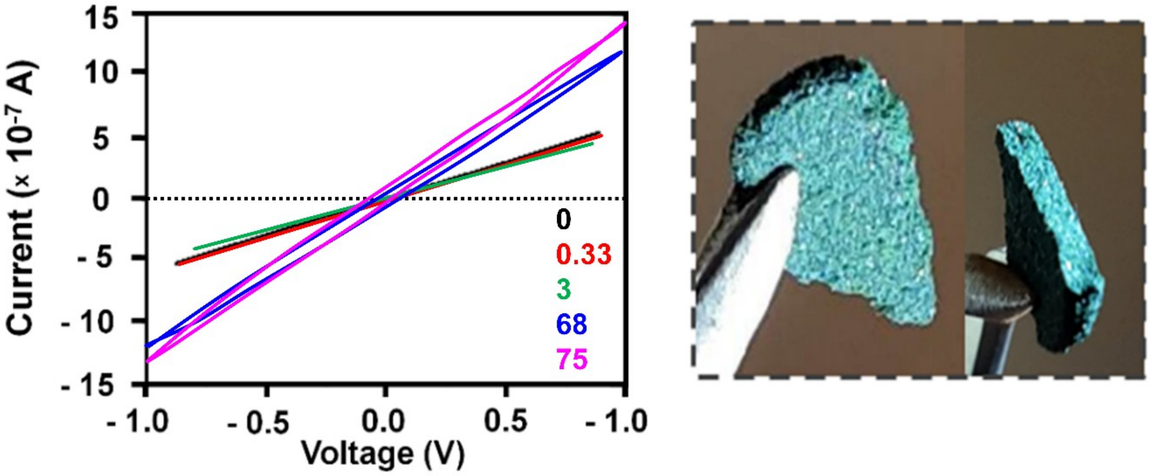

Figure S9. I-V graphs of the TCNQ@HKUST-1 host-guest composite material after different times: 0 (black), 0.33 (red), 3 (green), 68 (blue) and 75 h (pink); of exposure to air atmosphere. Image in the inset shows the powdered pellets used for conductivity measurements.

7. Nyquist Plots obtained from Electrochemical Impedance Spectroscopy (EIS)

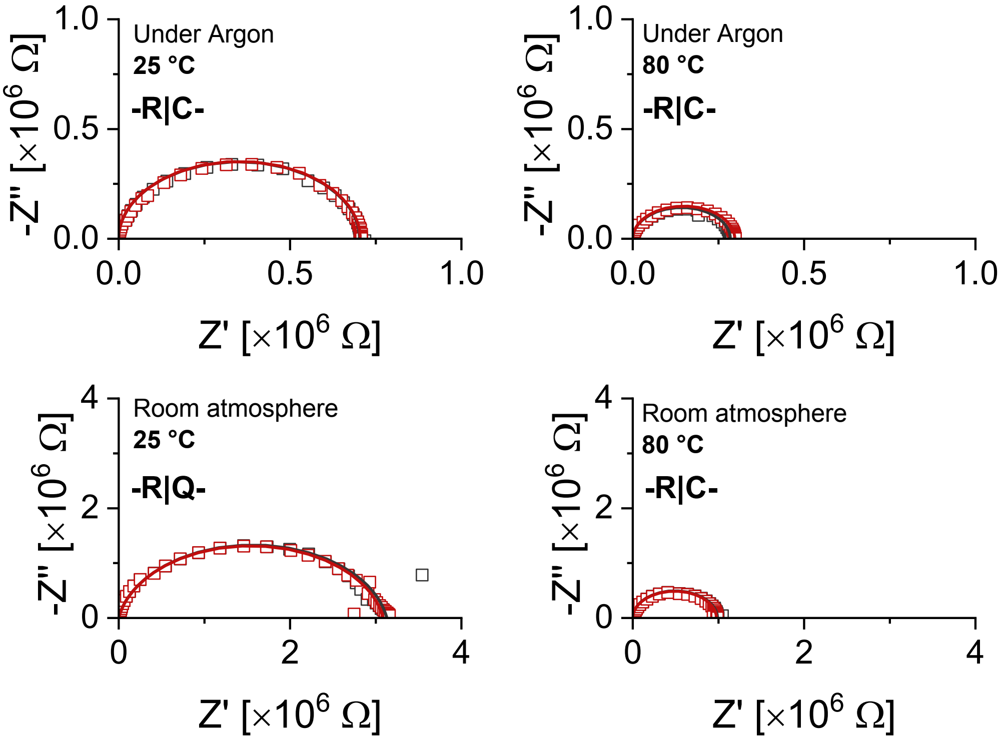

Figure S10. Nyquist plots of the electrochemical impedance spectroscopy (EIS) scans of TCNQ@HKUST-1. Collected data points (open squares) and fit (line). The equivalent circuit used to fit the data is given in each plot.

8. X-ray Photoelectron Spectroscopy (XPS) of TCNQ@HKUST-1

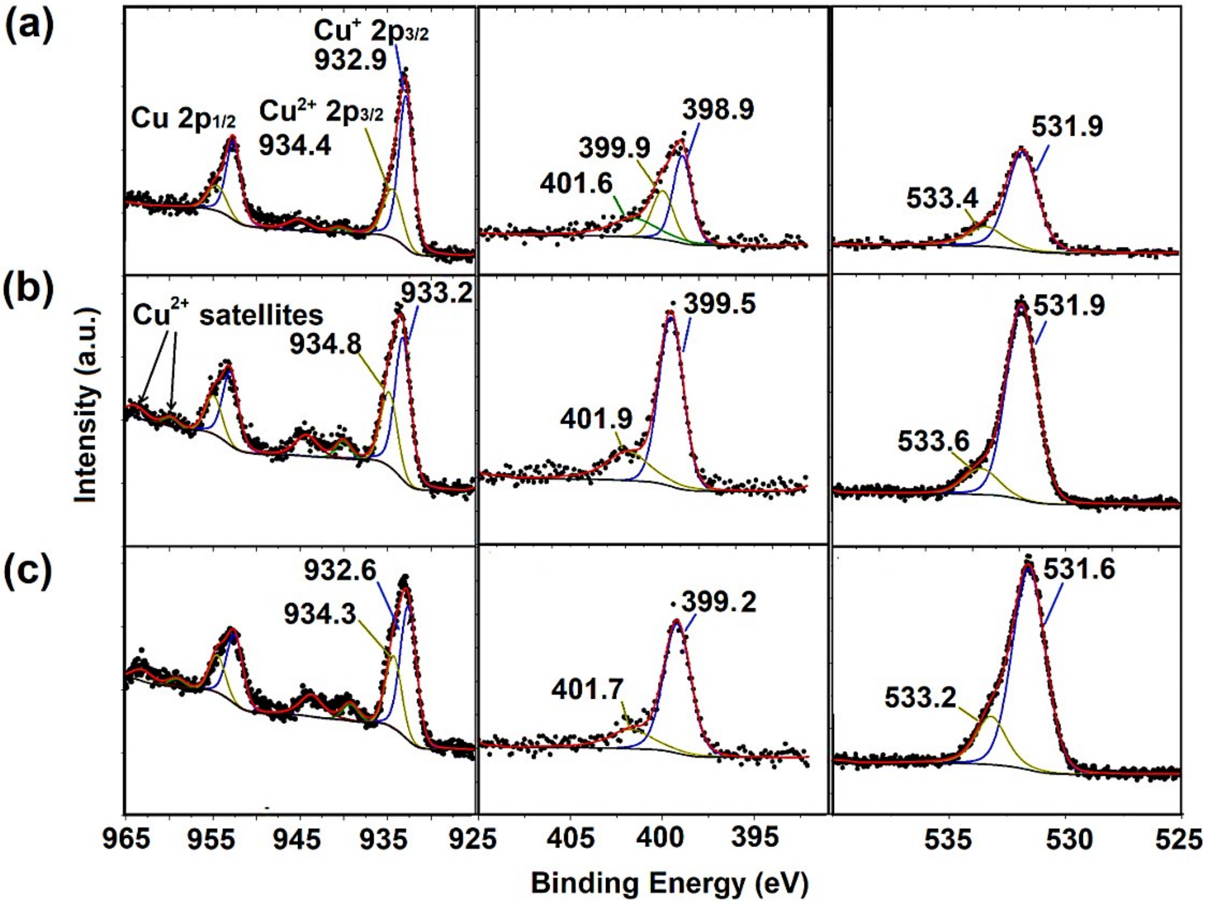

Figure S11. Core level X-ray Photoelectron Spectroscopy (XPS) data of the Cu 2p (left), N 1s (middle) and O 1s (right) for TCNQ@HKUST-1 host-guest composite material (a) before, (b) after measuring electrochemical impedance and (c) after water sorption experiments.

Reference

1. C. Schneider, D. Ukaj, R. Koerver, A. A. Talin, G. Kieslich, S. P. Pujari, H. Zuilhof, J. Janek, M. D. Allendorf and R. A. Fischer, *Chem. Sci.*, 2018, **9**, 7405-7412.